A complete framework for acousto-electric tomography with numerical examples

Changyou Li, An Kang, Kuisong Zheng, Dominique Lesselier

IEEE Access
Multidisciplinary | Rapid Review | Open Access Journal

Received February 12, 2020, accepted May 1, 2020, date of publication May 12, 2020, date of current version June 5, 2020.

Digital Object Identifier 10.1109/ACCESS.2020.2994153

A Complete Framework for Acousto-Electric Tomography With Numerical Examples

CHANGYOU LI[1], (Member, IEEE), KANG AN[1], KUISONG ZHENG[1], (Member, IEEE), AND DOMINIQUE LESSELIER[2], (Senior Member, IEEE)

[1]Department of Electronic Engineering, Northwestern Polytechnical University, Xi'an 710072, China
[2]Laboratoire des signaux et systèmes, CNRS, CentraleSupélec, Université Paris-Saclay, 91190 Gif-sur-Yvette, France

Corresponding author: Changyou Li (changyou.li@nwpu.edu.cn)

This work was supported by the National Natural Science Foundation of China under Grant 61801388 and Grant 61971351.

ABSTRACT Acousto-electric tomography (AET) involves three steps to retrieve the distribution of conductivity in a domain of interest (DOI): measure the potential on the DOI boundary (usually with a limited number of electrodes set there), compute the power density from this potential, use it to retrieve the distribution sought after. Almost all developed algorithms for AET assume that the power density is known, so their focus is mostly on the last step. A complete framework for AET is proposed herein to connect the three steps, the complete electrode model (CEM) being used to simulate the voltages measured on electrodes. The potential on the whole DOI boundary is reconstructed from such voltages. Then, the power density is computed, and the conductivity distribution in the DOI retrieved. A method based on singular value decomposition (SVD) is proposed. This method and the iterative Levenberg-Marquardt method are used for numerical illustration. The SVD-based method yields the potential on the whole DOI boundary, and a gross map of the conductivity distribution is also obtained, to serve as initial guess of the Levenberg-Marquardt method to yield the conductivity contribution with higher accuracy.

INDEX TERMS Acousto-electric tomography, electrical impedance tomography, complete electrode model, singular value decomposition, Levenberg-Marquardt method.

I. INTRODUCTION

Electrical impedance tomography (EIT) has attractive applications in medical imaging [1]–[3]. In the measurement, a number of electrodes are placed at the boundary of the domain of interest (DOI) and a given electrical current is injected between a pair of electrodes. The potentials on the other electrodes are then measured. It goes on likewise for every pair, and the corresponding measurements then yield a whole set of data which can be used to produce an image of the electrical conductivity distribution within the DOI, two-dimensional at least if proper symmetries or simplifications, three-dimensional at best. However, the total number of measurements is still much smaller than the number of points to reconstruct, thus EIT is an ill-posed inverse problem, and the spatial resolution remains low compared to other medical imaging methods.

The associate editor coordinating the review of this manuscript and approving it for publication was Ge Wang.

Some hybrid imaging methods [2] have been developed to overcome ill-posedness of electrical impedance tomography (EIT) and to correspondingly improve the image quality [3]. Other methods, e.g., learning structural sparsity via a Bayesian approach [4], [5] and some based on multi-physics models [6], [7] exist as well. AET is applied to determine the internal conductivity of a physical body with better stability and resolution compared to the ill-posed EIT. The main idea is to carry out a classical EIT measurement while a known focused ultrasonic wave travels through the DOI. The high intensity of the pressure produced by the acoustic wave creates a small local deformation within the DOI, and this deformation locally changes the electrical conductivity, hence the electrical current distribution which further changes the electric voltages measured on the electrodes. The higher the electrical conductivity in the acoustic wave focal zone, the larger the change. This deformation also influences the resolution of the imaging [1]. The resulting changes of the boundary potential can be recorded with EIT measurements [8], which are then

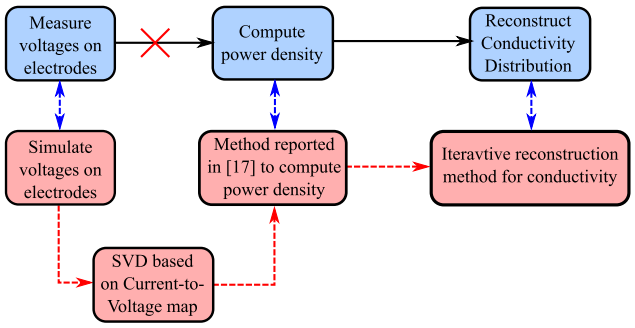

FIGURE 1. The three steps for AET and the complete framework for AET proposed in this contribution.

used to compute the power density [1], [9] for conductivity reconstruction.

There are three steps in AET to retrieve the conductivity in the DOI as well-known: measure the potential on the DOI boundary; compute the power density from this potential; use it to reconstruct the distribution of conductivity in the DOI. This is sketched in Fig. 1. In the second step, the reconstruction of the power density can be achieved from potentials on the whole DOI boundary, following [1]. Yet a limited number of electrodes is set in practice on the DOI boundary [9], and only their voltages are measured. That is, the second step cannot be achieved directly, since one needs to retrieve the potential on the whole DOI boundary before computing the power density.

In the existing literature, almost all applications of algorithms for AET consider that the power density is known, so focus is mostly on the third step of AET as investigated earlier in [10]–[12]. In the present contribution, all three steps are considered, CEM being used to simulate the measured voltages on electrodes since it appears as the model that provides simulated data best matching measured ones [9].

In a previous work [10], it was shown that the boundary potential converges much faster compared to the convergence rate of the conductivity in an iterative reconstruction process for EIT or AET —mainly because the boundary voltages measured on the DOI boundary are not sensitive to the interior changes of conductivity, e.g., [8]. This enabled to accelerate the convergence of the optimization procedure for the AET based on CEM and the Levenberg-Marquardt algorithm, a good performance being achieved.

In the present contribution, this observation has led to a method to reconstruct the boundary potential from an EIT measurement (voltages on a limited number of electrodes), which provides the necessary data to compute the power density for the retrieval of the conductivity in the DOI. In doing so, the aforementioned second step is completed, and hence a complete framework for AET follows.

To illustrate the feasibility of the proposed framework for AET, the CEM is used to simulate the voltages on the electrodes. A method based on singular value decomposition (SVD) is proposed and applied to obtain the boundary potentials from the boundary voltages measured, a low-accuracy conductivity distribution being also obtained during this first step. The latter is taken as initial guess in the next step, a Levenberg-Marquardt method as discussed in [10], [13] yielding the conductivity distribution with high accuracy from the power density.

The contribution is organized as follows. In section II, the complete electrode model is introduced and a singular value decomposition method for EIT is investigated. The Levenberg-Marquardt method based on a continuum forward model is also presented. In Section III, numerical experiments are carried out. The proposed strategy is illustrated and validated with the methods introduced in the previous section. Conclusions and perspectives are in section IV.

II. RECONSTRUCTION ALGORITHMS

A DOI imaged by AET is modeled as a bounded Lipschitz domain $\Omega \subset \mathbb{R}^n$, $n \geq 2$. The changes caused by the acoustic wave can be recorded with EIT measurements on the boundary $\partial\Omega$ [14], [15]. The power density in Ω is defined as

$$\mathcal{E}(\sigma) = \sigma|\nabla u(\sigma)|^2, \quad \Omega \subset \mathbb{R}^n. \tag{1}$$

Here, σ is the conductivity distribution in domain Ω, and $u(\sigma)$ is the electrical potential produced by applying either voltage or electric current on $\partial\Omega$. Given noisy measurements $\mathcal{E}^\delta(\sigma)$ of the true power densities $\mathcal{E}(\sigma)$, the problem is to find the conductivity map σ by minimizing the functional

$$\min_{\sigma} ||\mathcal{E}^\delta(\sigma) - \mathcal{E}(\sigma)||_{L^2(\Omega)}. \tag{2}$$

$\mathcal{E}(\sigma)$ can be retrieved from the boundary measurements [1], [16]. Yet the non-linear relationship between $\mathcal{E}(\sigma)$ and σ renders this problem nonlinear [17].

The proposed strategy for AET is sketched in Strategy 1. Data $U_{l,\epsilon}$ and U_l are the measured voltages on the electrodes e_l, $l = 1, 2, \ldots, N$, with and without the perturbation of the focused ultrasonic wave, respectively. In this contribution, those are simulated with the CEM model, as the most practical model for EIT, and able to simulate the electrical potential with very good accuracy [18]. It is given with equations (3):

$$\nabla \cdot \sigma \nabla u = 0, \text{ in } \Omega, \tag{3a}$$

$$\sigma \frac{\partial u}{\partial \nu} = 0, \text{ on } \partial\Omega \backslash \bigcup_{l=1}^{L} e_l, \tag{3b}$$

$$\int_{e_l} \sigma \frac{\partial u}{\partial \nu} = I_l, \quad \text{on } e_l \text{ for } l = 1, \ldots, N, \tag{3c}$$

$$u + z_l \sigma \frac{\partial u}{\partial \nu} = U_l, \quad \text{on } e_l. \tag{3d}$$

N electrodes are attached at the boundary $\partial\Omega$. A known total current I_l is injected through the l-th electrode. Here, ν is the outward unit normal vector to boundary $\partial\Omega$, e_l the area occupied by the l-th electrode, and $\partial/\partial\nu$ indicates the directional derivative of u along ν, z_l being the contact impedance corresponding to the l-th electrode. To ensure existence and uniqueness of the solution, this model must include the law of

charge conservation: $\sum_{l=1}^{N} I_l = 0$, and $\sum_{l=1}^{N} U_l = 0$ is also required to uniquely determine the solution of (3). Replacing the boundary conditions (3b)-(3d) in equations (3) yields the continuum model.

It is assumed that the conductivity map $\sigma \in \mathcal{H}^s(\Omega)$ for $s > n/2$, where $\mathcal{H}^s(\Omega)$ is the Sobolev space. It implies that the Sobolev space $\mathcal{H}^s(\Omega)$ is a Banach algebra w.r.t point-wise multiplication [19]. The "discontinuous" Robin-type boundary conditions (3d) are such that the regularity of the CEM solution $u(\sigma)$ is limited in $\mathcal{H}^{2-\epsilon}(\Omega)$ [9] for $\epsilon > 0$, so $\mathcal{E}(\sigma) : \mathcal{H}^s(\Omega) \to \mathcal{H}^{1-\epsilon}(\Omega)$ with singularities at the edges of the electrodes —those can be eliminated with a contact impedance which exhibits smoothed value changes set at edges of the electrodes.

As indicated already, this step is performed with SVD. Potentials u_b and $u_{b,\epsilon}$ on the entire boundary of the DOI are retrieved from U_l and $U_{l,\epsilon}$, respectively, then the power density proceeds from u_b and $u_{b,\epsilon}$ by using the method introduced in [1].

Strategy 1: Proposed strategy for the retrieval of the conductivity distribution in the DOI from boundary measurements with a limited number of electrodes.

Data: Measured U_l and $U_{l,\epsilon}$ on electrodes e_l.
Result: The conductivity distribution σ_r in DOI.
1 determine u_b and σ_0 from U_l based on EIT;
2 determine $u_{b,\epsilon}$ and $\sigma_{0,\epsilon}$ from $U_{\epsilon,l}$ based on EIT;
3 determine $\mathcal{E}(\sigma)$ from u_b and $u_{b,\epsilon}$;
4 determine σ_r from $\mathcal{E}(\sigma)$ with σ_0 as initial guess.

A. RETRIEVAL OF u_b AND $\mathcal{E}(\sigma)$

With the electrodes configuration as in (3), the space

$$\mathbb{V}_\diamond = \text{span}\{\chi_1, \chi_2, \ldots, \chi_l\} \cap \mathcal{L}^2_\diamond(\partial\Omega) \subset \mathcal{L}^2_\diamond(\partial\Omega) \quad (4)$$

is introduced, letting $l = 1, \ldots, N$. Here χ_l is the indicator function of the l-th electrode and $\mathcal{L}^2_\diamond(\partial\Omega) = \{f \in \mathcal{L}^2(\partial\Omega) : \int_{\partial\Omega} f = 0\}$. The weak formulation of the CEM reads [18]

$$a((u, U), (v, V)) = \int_{\partial\Omega} IV, \quad (5)$$

where

$$a((u, U), (v, V)) := \int_\Omega \sigma \nabla u \nabla v \mathrm{d}x + \frac{1}{z}\int_e (u - U)(v - V) \quad (6)$$

is a bilinear form $a((u, U), (v, V)) : \mathbb{U} \oplus \mathbb{V}_\diamond \times \mathbb{U} \oplus \mathbb{V}_\diamond \to \mathbb{R}$ with $u, v \in \mathbb{U}$. It is assumed $\mathbb{U} = H^1(\Omega)$ herein. As CEM only provides $N(N-1)/2$ independent measurements, conductivities can only be recovered to a degree-of-freedom less than the number of independent measurements. The forward CEM can be represented with current-to-voltage map

$$T : \mathbb{B}(\mathbb{S}^+_{\mathcal{T}_\sigma}, \mathbb{V}_\diamond) \to (\mathbb{U}_{\mathcal{T}_u}, \mathbb{V}_\diamond) \quad , T(\sigma, I) = (u, U) \quad (7)$$

with $I, U \in \mathbb{V}_\diamond$. Let $\mathbb{S}^+ = \{\sigma \in \mathbb{S} : \sigma \geq c_0, c_0 > 0\}$, with $\sigma = \sigma_0 + h$, $h \in L^\infty(\Omega)$ being a small perturbation, and $\sigma_0 \in \mathbb{S}^+$ as background conductivity in the DOI. Linearizing around σ_0 yields

$$T(\sigma_0 + h, I) = T(\sigma_0, I) + T'(\sigma_0, I)[h] + o(h), \quad (8)$$

which enables to predict the influence of h. Here, $T'(\sigma, I)[h]$ is the Fréchet derivative of $T(\sigma, I)$ along the direction h. Due to the symmetry of $T(\sigma_0, I)$, easily validated by $\langle T(\sigma_0, I), J\rangle_{L^2_\diamond} = \langle J, T(\sigma_0, I)\rangle_{L^2_\diamond}$ with (5), the map $T(\sigma, I)$ is represented with a symmetric matrix in the order of dimension $N - 1$, written as

$$[\mathbf{T}_\sigma]_{i,j} = \langle T(\sigma, I_i), I_j\rangle, \quad (9)$$

where I_i and I_j are the ith and jth column vectors of an orthonormal basis $\mathbf{I}$ of $\mathbb{V}_\diamond$. The Fréchet derivative $T'(\sigma_0, I)[h]$ is thus represented in matrix form [20] as

$$T'(\sigma_0, I)[h] = -\int_\Omega h \nabla u(I_i) \nabla u(I_j) dx, \quad (10)$$

$u(I_i)$ as unique solution of (5) w.r.t. the electrode current I_i.

In numerical settings, Ω can be described via a triangulation $\mathcal{T}$, so as (10) is approximated by

$$T'(\sigma_0, I)[h] \approx -\sum_{t\in\mathbb{T}} h_t \int_t \nabla u(I_i) \nabla u(I_j) dx \quad (11)$$

with the assumption that h is a constant in triangle t. If T triangles in the mesh $\mathbb{T}$, (11) is written in a $(N-1)^2 \times T$ matrix form with

$$\left[\mathbf{T}'\right]_{k,t} = -\int_t \nabla u(I_i) \nabla u(I_j) dx, \quad k = i(N-1) + j. \quad (12)$$

With (9) and (12), (8) can be written into a linear system

$$\mathbf{T}'\mathbf{h} = \mathbf{b} \quad (13)$$

with $\mathbf{h} = \{h_1, h2, \ldots, h_T\}$, and $\mathbf{b}$ a vector obtained via reshaping the matrix $\mathbf{T}_{\sigma_0+h} - \mathbf{T}_{\sigma_0}$. $\mathbb{S}^+_{\mathcal{T}_\sigma} = \{\sigma \in \mathbb{S}_\mathcal{T} : \sigma \geq c_0, c_0 > 0\}$.

The conductivity distribution can be obtained with an iterative algorithm [21] or singular value decomposition, as herein. In vector form, the reconstructed perturbation h_r is

$$\mathbf{h}_r = \sum_{i=1}^{N} \frac{\langle \mathbf{b}, \mathbf{u}_i\rangle}{s_i} \mathbf{v}_i. \quad (14)$$

Here, s_i are singular values of $\mathbf{T}'$, $\mathbf{u}_i$ and $\mathbf{v}_i$ the corresponding singular vectors, N the number of singular values used. With $\mathbf{h}_r$, the boundary potential u_b can be obtained by solving (5) with $\sigma_r = \sigma_0 + h_r$.

With the perturbation ϵ introduced by the focused ultrasonic wave, the boundary potential $u_{b,\epsilon}$ can be retrieved as the one for u_b. According to [1], the power density can in principle be obtained from u_b and $u_{b,\epsilon}$ with

$$\mathcal{E}(\sigma) = \left(\int_\omega \frac{(\nu(x) - 1)^2}{\nu(x) + 1} \mathrm{d}x\right)^{-1} \int_{\partial\Omega} (u_{b,\epsilon} - u_b)\phi_I, \quad (15)$$

where $\nu(x)$ is the ratio between perturbed and original volumes, and where ϕ_I is the current distribution on the boundary of the DOI, both of them being known functions.

B. RETRIEVAL OF σ FROM $\mathcal{E}(\sigma)$

An iterative method based on the Levenberg-Marquardt algorithm (LMA) [22]–[24], as a well-known solution method for non-linear least-square problems, can yield the distribution of σ from $\mathcal{E}(\sigma)$. LMA locates the minimum of a function expressed as the sum of squares of errors between function and measured data through iterative updating. For a general operator equation $F(\sigma) = \mathcal{E}(\sigma)^\delta$, where $F : X \to Y$ and X, Y are Hilbert spaces. $\mathcal{E}(\sigma)^\delta$ is the measured noisy data of $\mathcal{E}(\sigma)$. More practical, one could instead minimize [25]

$$\sigma_{k+1} = \min_{\sigma} \left\| \mathcal{E}(\sigma)^\delta - F(\sigma_k) - F'(\sigma_k)\delta\sigma \right\|_Y^2 + \alpha_k \left\| \delta\sigma \right\|_X^2, \tag{16}$$

letting α_k be the Tikhonov regularization parameter, and $\delta\sigma = \sigma - \sigma_k$. This minimization problem regarding to (16) is equivalent to the linearized one

$$\sigma_{k+1} = \sigma_k (F'(\sigma_k)^* F'(\sigma_k) + \alpha_k)^{-1} F'(\sigma_k)^* (\mathcal{E}(\sigma)^\delta - F(\sigma_k)), \tag{17}$$

letting $F'(\sigma_k)^*$ be the adjoint of $F'(\sigma_k)$. In [13] and [24], It has been proven that, with properly chosen parameter α_k and an initial guess σ_0 sufficiently close to the desired solution, the LMA converges to a solution σ^δ of $F(\sigma^\delta) = \mathcal{E}(\sigma)^\delta$.

The LMA based on (17) can be seen as a combination of steepest descent and Gauss-Newton method. When the current solution is far from the correct one, a large value is given to α_k, and it behaves like a steepest-descent method which converges slowly but well. When the current solution is close to the correct solution, a small α_k is used, and it behaves like a Gauss-Newton method, which is faster than the steepest descent. This method is used here for our fourth step in Strategy 1. The Fréchet derivative and adjoint operator needed in (17) are computed with a method proposed in [13], as follows. It is assumed that σ is positive, and $\sigma \in \mathcal{H}^l(\Omega)$ for $l > n/2$. For $f \in \mathcal{H}^{l+\frac{1}{2}}(\Omega)$, then (3) has a unique solution $u(\sigma) \in \mathcal{H}^{l+1}(\Omega)$, which indicates that the operators $\mathcal{E}(\sigma)$, $\mathcal{E}'(\sigma)$ and $\mathcal{E}'(\sigma)^*$ are all maps from $\mathcal{H}^s(\Omega)$ to $\mathcal{H}^s(\Omega)$ [13].

If $u'(\sigma)$ is the Fréchet derivative of $u(\sigma)$ in Ω,

$$u(\sigma + \tau) = u(\sigma) + u'(\sigma)\tau + o(\tau) \tag{18}$$

is established for $\tau \to 0$, $o(\tau)$ as the remainder. Define $L_\sigma(u) = u \to \nabla \cdot (\sigma \nabla u)$. According to (3a) and (18),

$$L_\sigma u'(\sigma)\tau + \nabla \cdot (\tau \nabla u(\sigma)) = 0. \tag{19}$$

The boundary conditions for $u'(\sigma)\tau$ can also be derived from (3a) by using (18). If $\xi = u'(\sigma)\tau$, then ξ satisfies

$$\nabla \cdot \sigma \nabla \xi + \nabla \cdot (\tau \nabla u(\sigma)) = 0, \quad \text{in } \Omega, \tag{20a}$$
$$\xi = 0, \quad \text{on } e_l. \tag{20b}$$

Here, it is assumed that τ vanishes in a domain $\Omega_\epsilon = \{x \in \bar{\Omega} | d(x, \partial\Omega) < \epsilon\}$ for a sufficiently small ϵ. So, all terms associated to τ in the boundary conditions disappear. It is well-known that the solution of equations (20) uniquely exists in the weak sense. $u'(\sigma)$ as defined in (20) is the Fréchet derivative of $u(\sigma)$.

The directional derivative of $\mathcal{E}(\sigma)$ is given as

$$\mathcal{E}'(\sigma)\tau \approx \mathcal{E}(\sigma + \tau) - \mathcal{E}(\sigma) \approx \tau |\nabla u(\sigma)|^2 + 2\sigma \nabla u(\sigma) \nabla \xi, \tag{21}$$

terms of the order of $\|\tau\|^2$ being neglected. $\mathcal{E}'(\sigma)\tau$ is actually the Fréchet derivative of $\mathcal{E}(\sigma)$.

Let us take $\Omega \subset \mathbb{R}^2$ for simplicity, and consider the noise effect. The latter cannot be assumed differentiable, then $\mathcal{E}(\sigma) : \mathcal{H}^2(\Omega) \to \mathcal{L}^2(\Omega)$. Since $\mathcal{E}'(\sigma) : \mathcal{H}^2(\Omega) \to \mathcal{L}^2(\Omega)$ is a bounded operator, its Hilbert adjoint $\mathcal{E}'(\sigma)^* : \mathcal{L}^2(\Omega) \to \mathcal{H}^2(\Omega)$ is bounded [26]. Upon introduction of the embedding operator $B : \mathcal{H}^2(\Omega) \to \mathcal{L}^2(\Omega)$, $\mathcal{E}'(\sigma)^*$ can be written as

$$\mathcal{E}'(\sigma)^* : \mathcal{L}^2(\Omega) \to \mathcal{H}^2(\Omega), \tag{22}$$
$$\mathcal{E}'(\sigma)^* z = B^* \tilde{\mathcal{E}}'(\sigma)^* z. \tag{23}$$

$\tilde{\mathcal{E}}'(\sigma)^*$ is the $\mathcal{L}^2(\Omega)$-adjoint of $\mathcal{E}'(\sigma)$. $z \in \mathcal{L}^2(\Omega)$, and $\tilde{\mathcal{E}}'(\sigma)^* z = |\nabla u(\sigma)|^2 z + 2\nabla u \nabla V z$. The map $V : \mathcal{H}^2(\Omega) \to \mathcal{H}^2(\Omega)$ is linear and defined by

$$L_\sigma V z = -\nabla \cdot (z\sigma \nabla u(\sigma)) \quad \text{in } \Omega, \tag{24a}$$
$$V z = 0 \text{ on } \partial\Omega. \tag{24b}$$

If multiple measurements are performed, $\tilde{\mathcal{E}}'_H(\sigma)^* z$ in (23) is replaced with $\tilde{\boldsymbol{\mathcal{E}}}'(\sigma)$ defined as

$$\tilde{\boldsymbol{\mathcal{E}}}'(\sigma)^* z = B^* \sum_{i=1}^{M} (|\nabla u_i(\sigma)|^2 z_i + 2\nabla u_i \nabla V z_i). \tag{25}$$

To calculate $B^* : \mathcal{L}^2(\Omega) \to \mathcal{H}^2(\Omega)$, one allows

$$\sigma \in H_0^2(\Omega) = \left\{ x \in \mathcal{H}^2(\Omega) : \frac{\partial x}{\partial \nu} = 0 \right\} \tag{26}$$

with its inner product given as

$$\langle x, y \rangle_{\mathcal{H}^2(\Omega)} = \langle x, y \rangle_{\mathcal{L}^2(\Omega)} + \beta^2 \langle \Delta x, \Delta y \rangle_{\mathcal{L}^2(\Omega)}. \tag{27}$$

β is a regularization parameter. Upon integration by parts, $B^*\zeta$ is the solution of the Neumann problem

$$(Id + \beta^2 \Delta\Delta) B^* \varsigma = \varsigma, \tag{28a}$$
$$\frac{\partial \Delta B^* \varsigma}{\partial \nu} = 0, \quad \text{on } \partial\Omega \tag{28b}$$
$$\frac{\partial B^* \varsigma}{\partial \nu} = 0, \quad \text{on } \partial\Omega \tag{28c}$$

with $\varsigma \in \mathcal{L}^2(\Omega)$. Refer to [13] for more detail. This fourth-order partial differential equation is not practical, but it can be written into an equivalent form:

$$B^* \varsigma + \beta^2 \Delta \chi = \varsigma, \tag{29a}$$
$$\chi - \Delta B^* \varsigma = 0, \tag{29b}$$
$$\frac{\partial \chi}{\partial \nu} = 0, \quad \text{on } \partial\Omega, \tag{29c}$$
$$\frac{\partial B^* \varsigma}{\partial \nu} = 0, \quad \text{on } \partial\Omega. \tag{29d}$$

According to the Levenberg-Marquardt iteration in (17), the formula for calculating the k-th updating step τ_k for the problem at hand is given as

$$(\mathcal{E}'(\sigma_k)^*\mathcal{E}'(\sigma_k) + \alpha_k Id)\tau_k = \mathcal{E}'(\sigma_k)^*(\mathcal{E}^\delta - \mathcal{E}(\sigma_k)), \quad (30)$$

where $\mathcal{E}^\delta$ represents the measured power density derived from u_b and $u_{b,\epsilon}$ in the last section. For the left hand side of (30), $\mathcal{E}'(\sigma_k)^*\mathcal{E}'(\sigma_k)\tau = B^*M\tau$ with

$$M\tau = |\nabla u|^2(\tau|\nabla u|^2 + 2\sigma\nabla u\nabla u'(\sigma)\tau) + 2\nabla u\nabla V(\tau|\nabla u|^2) + 4\nabla u\nabla V(\sigma\nabla u\nabla u'(\sigma)\tau). \quad (31)$$

Here, $M\tau$ is easily obtained with (21), (23). After computing τ_k from (30), the conductivity map σ_k obtained at the k-th iteration is updated by $\sigma_{k+1} = \sigma_k + \tau_k$ for a new iteration. To calculate $B^*M\tau$, equation (29) has to be solved with $\varsigma = M\tau$, which requires first solving (20) and (24). Since all these PDE systems are coupled to one another via τ, they need to be collected into one PDE system and solved in one variational form.

This yields the following system

$$\begin{aligned}
\phi + \alpha_k\tau_k &= y, && \text{in } \Omega, && (32a)\\
\Delta\phi - \chi &= 0, && \text{on } \partial\Omega, && (32b)\\
\beta^2\Delta\chi + \phi - \gamma &= 0, && \text{on } \partial\Omega, && (32c)\\
\partial\phi/\partial\nu &= 0, && \text{on } \partial\Omega && (32d)\\
\partial\chi/\partial\nu &= 0, && \text{on } \partial\Omega && (32e)\\
\gamma - M\tau &= 0, && \text{in } \Omega, && (32f)\\
\nabla\cdot(\sigma+\tau)\nabla\xi + \nabla\cdot(\tau\nabla u(\sigma)) &= 0, && \text{in } \Omega, && (32g)\\
\xi &= 0, && \text{on } \partial\Omega, && (32h)\\
L_\sigma\rho + \nabla\cdot(\Phi_\epsilon(\tau|\nabla u|^2)\sigma\nabla u(\sigma)) &= 0, && \text{in } \Omega, && (32i)\\
\rho &= 0, && \text{on } \partial\Omega && (32j)\\
L_\sigma\kappa + \nabla\cdot(\Phi_\epsilon(\sigma\nabla u\nabla\xi)\sigma\nabla u(\sigma)) &= 0, && \text{in } \Omega, && (32k)\\
\kappa &= 0, && \text{on } \partial\Omega. && (32l)
\end{aligned}$$

with $y = \mathcal{E}'(\sigma_k)^*(\mathcal{E}^\delta - \mathcal{E}(\sigma_k))$, $\phi = B^*M\tau$, $\rho = V(\tau|\nabla u|^2)$, and $\kappa = V(\sigma\nabla u\nabla u'(\sigma)\tau)$. If the number of measurements $N > 1$, $y = \boldsymbol{\mathcal{E}}(\sigma_k)^*(\boldsymbol{\mathcal{E}}^\delta - \boldsymbol{E}(\sigma_k))$ and $\gamma = \sum_n^N M_n\tau$ with

$$M_n\tau = |\nabla u_n|^2(\tau|\nabla u_n|^2 + 2\sigma\nabla u_n\nabla\xi_n) + 2\nabla u_n\nabla\zeta_n + 4\nabla u_n\nabla\kappa_n. \quad (33)$$

Equations (32g)-(32l) must be solved for each measurement, so one additional measurement will require to solve in addition three partial differential equations. The smoothness requirement on σ can be achieved by a so-called mollification operation. To solve the above system, $\mathcal{E}'(\sigma_k)^*(\mathcal{E}^\delta - \mathcal{E}(\sigma_k))$ is needed first. Let $g = \mathcal{E}^\delta - \mathcal{E}(\sigma_k)$, then $\mathcal{E}'(\sigma_k)^*g = B^*z$ with $z = |\nabla u|^2\Phi_\epsilon g + 2\nabla u\nabla w$ and $h = V\Phi_\epsilon g$. Thus, w can be calculated with (24), and $x = B^*z$ is the solution of (29).

The iterative construction method based on the above system is named as LM-CM, refer to Algorithm 2 for a single measurement. Since $\nu(x)$ is not known for the current numerical study, the data of $\mathcal{E}^\delta$ are simulated by solving (3a) with Dirichlet boundary condition $u = u_b$ in the present contribution. The relative error η is defined as $\eta = \|\sigma_t - \sigma_r\|_{L_2}/\|\sigma_t\|_{L_2}$. Index t indicates the true value, and r means retrieved value. The parameter α_k should be updated according to the value of τ_k. If $\sigma_k + \tau_k$ leads to a reduction of the relative error in σ_k, α_k is decreased and τ_k is accepted. Otherwise, τ_k is discarded and α_k is increased. Since η cannot be determined in practice, a relatively large value can be given to α_0, and α_k slowly decreased to ensure convergence. The iteration is stopped if $\|\tau_k\|_{L_2}$ is smaller than the expected error or if the maximum number of iterations is reached.

Algorithm 2: LM-SCEM Algorithm for Retrieving the Conductivity Map of a Domain Ω From a Single Measurement of Power Density

Data: Measured power density $\mathcal{E}^\delta$ and initial guess σ_0
Result: Retrieved conductivity map σ_r with relative error η

N: maximum number of iterations;
$\sigma_k \leftarrow \sigma_0$;
$\alpha_k \leftarrow \alpha_0$;
$num \leftarrow 1$;
$norm \leftarrow 1$;
while $norm > \delta$ *and* $num < N$ **do**
  Update u_k from σ_k with CEM;
  Compute $\mathcal{E}(\sigma_k)$ from u_k;
  Compute $y = \mathcal{E}'(\sigma_k)^*(\mathcal{E}^\delta - \mathcal{E}(\sigma_k))$ with (24) and (29);
  Compute τ_k with the linear system defined by (32);
  $\sigma_k \leftarrow \sigma_k + \tau_k$;
  $norm \leftarrow \|\tau_k\|_{L_2}$;
  $num \leftarrow num + 1$;
  Update α_k;
end

III. NUMERICAL INVESTIGATION

A. THE PHANTOM USED IN THE SIMULATION

The numerical experiments are carried out with a lung-heart model depicted in Fig. 2a. Three tissues are considered: heart (red, $\sigma = 0.7\,\mathrm{S/m}$), lung (cyan, $\sigma = 0.26\,\mathrm{S/m}$), and soft-tissues (blue, $\sigma = 0.33\,\mathrm{S/m}$). The model is in a circular region with background material (white, $\sigma = 0.20\,\mathrm{S/m}$) and radius $r = 23\,\mathrm{cm}$. So, the conductivity distribution of the phantom is piecewise. The boundaries between two regions with different conductivities are smoothed via a convolution between conductivity distribution and mollification equation

$$\eta_\epsilon(x, y) = C\exp\left(\frac{\epsilon^2}{(x^2+y^2)-\epsilon^2}\right), \quad (34)$$

which reduces interpolation errors at the boundaries. The mollified conductivity distribution of the model is displayed in Fig. 2b,, and it is referred to as σ_0. All electrodes are uniformly distributed on the boundary of the DOI, indicated as the red squares in Fig. 2a.

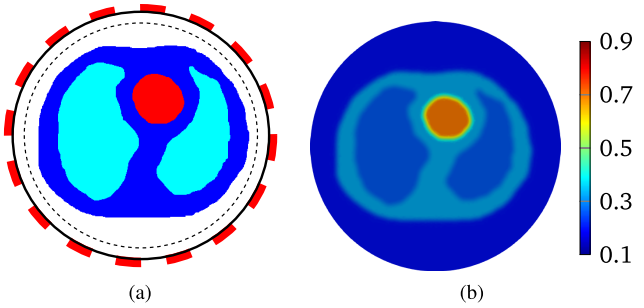

FIGURE 2. The model used in numerical investigations: (a) Heart-lung model. (b) Conductivity σ_0 without perturbation.

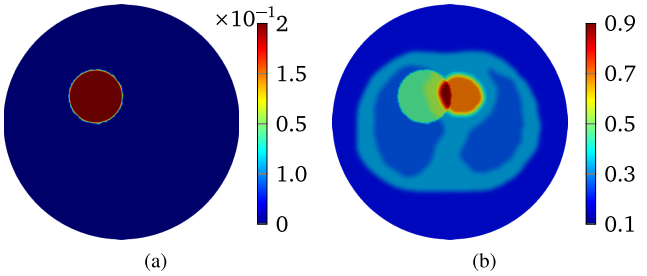

FIGURE 3. (a) The perturbation introduced into the heart-lung model. (b) Conductivity distribution of perturbed model.

A perturbation h, refer to Fig. 3(a), is introduced in the model. The perturbation value in the red circular domain is given as 0.2 S/m, and the values in other parts are all zero. The conductivity distribution of the perturbed model is shown in Fig. 3(b), which is simple $\sigma_0 + h$. The relative error of the reconstruction is defined ccording to the L_2 norm, $\delta = \frac{\|h_t - h_r\|_{L_2}}{\|h_t\|_{L^2}}$. h_t and h_r are the true and retrieved distributions of perturbation function h. Simulations are all carried out with 32 electrodes.

B. RECONSTRUCTION OF u_b AND $\mathcal{E}(\sigma)$ WITH SVD-BASED METHOD

Following the steps in Strategy 1, the SVD-based method introduced in section III provides the perturbation h from the measured voltage on the electrodes as attached on the boundary. The DOI given in Fig. 2a is meshed with 14163 triangular elements, yielding a matrix $\mathbf{T}'$ of dimensions 961 × 14163 since 32 electrodes. The current pattern used in the example is set as

$$I_l^n = \begin{cases} M\cos(n\theta_l), & n = 1, \ldots, \frac{L}{2} - 1 \\ M\cos(\pi l), & n = L/2 \\ M\sin((n - L/2)\theta_l), & n = L/2 + 1, \ldots, L - 1, \end{cases} \tag{35}$$

where M is the (maximum) current amplitude. The vector I^n is a current pattern, which is a discrete approximation to $M\cos(n\theta)$ for $1 < n < L/2$ or $M\sin(n\theta)$ for $L/2 - 1 \leq n \leq L - 1$. The vectors I^n are orthonormalized to form a complete set of bases for the space $\mathbb{V}_\diamond$. After computing the matrices $\mathbf{T}_{\sigma_0+h}$, $\mathbf{T}_{\sigma_0}$ and $\mathbf{T}'$ from the data obtained with the complete electrode model, the vector $\mathbf{h}$ can be computed from (14).

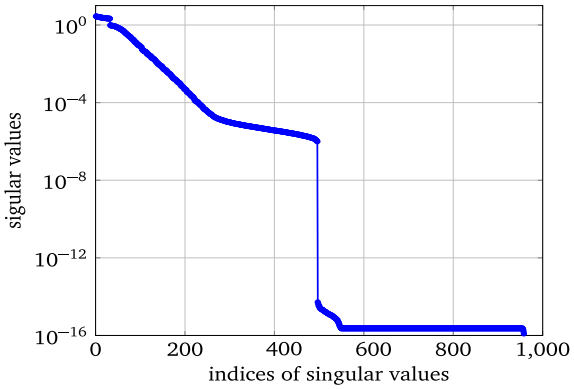

FIGURE 4. The T′ matrix: distribution of its singular values.

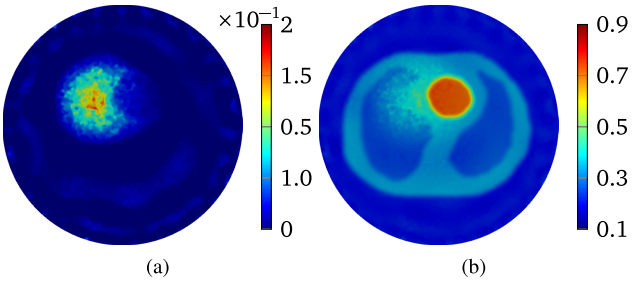

FIGURE 5. (a) Reconstructed distribution of h. (b) Reconstructed perturbed distribution of σ.

The singular values of the matrix $\mathbf{T}'$ are ordered from large to small and shown in Fig. 4. Generally, the singular vectors associated to the large ones give more information about the region close to the DOI boundary, and those assocoated to the smaller ones give more information about the interior region. However, if the singular value s_i is too small, a very large influence will be put on h_r since s_i is at the denominator of (14). Thus, only a limited number of singular values is used to reconstruct h_r.

The variation of the relative error δ with the number of singular values employed in the reconstruction is shown in Fig.6. The best results are obtained by using the first 175 largest singular values with relative error $\delta = 0.6141$. The retrieved h in the DOI is shown in Fig. 5a. Obviously, position and profile of the perturbation can be suitably retrieved with the SVD-based method, but the relative error is not good enough for a good reconstruction of h_r. This is mainly caused by the Robin-type boundary condition applied in the CEM. This leads to the computed potential existing in $H^{2-\epsilon}$ when $\sigma \in H^2$, thus the computed power density $\mathcal{E}(\sigma_k)$ is in $H^{1-\epsilon}$ for any $\epsilon > 0$. In particular they are not in H^ϵ with $\epsilon > n/2$ even in one dimension [27], [28]. Yet, it will be shown below that the value obained is good enough for determination of the boundary potential u_b.

To verify that the measured boundary potential in EIT is not very sensitive to the changes of the interior conductivity, the boundary potentials for the perturbed conductivity map $\sigma_{p,t}$ and the retrieved one $\sigma_{p,r}$ are computed using

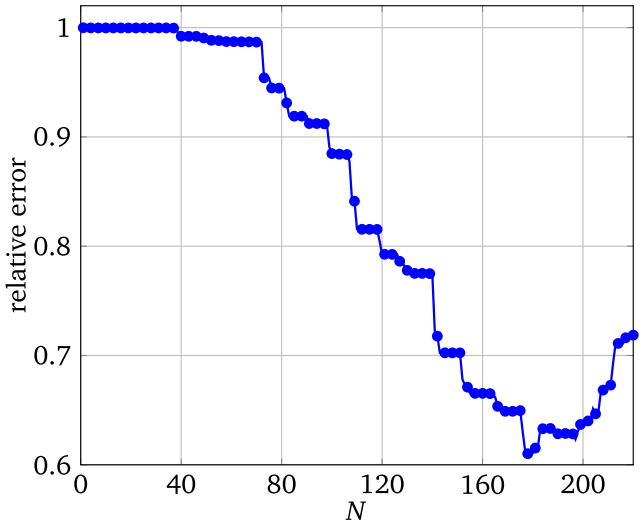

FIGURE 6. Variation of the relative error with the number of singular values in the SVD-based reconstruction method.

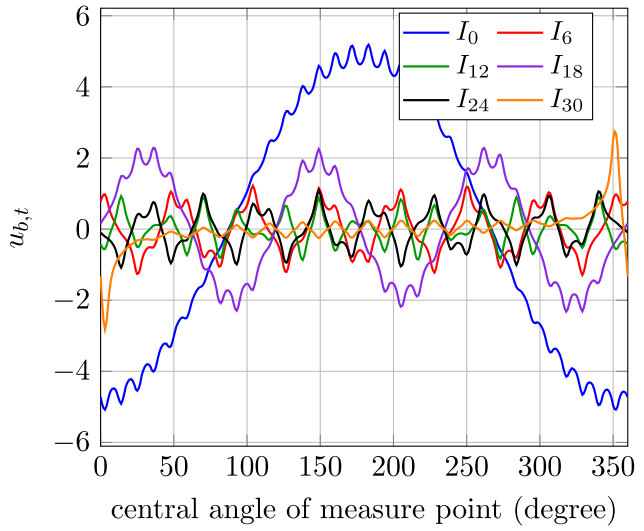

FIGURE 7. Boundary potential for different current patterns.

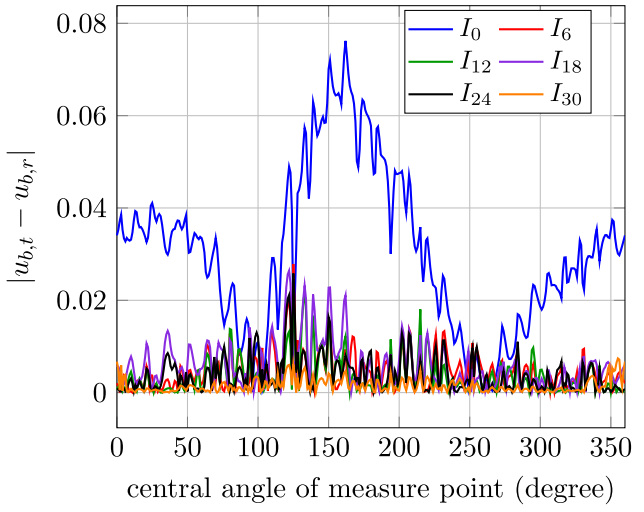

FIGURE 8. Difference between $u_{b,t}$ and $u_{b,r}$.

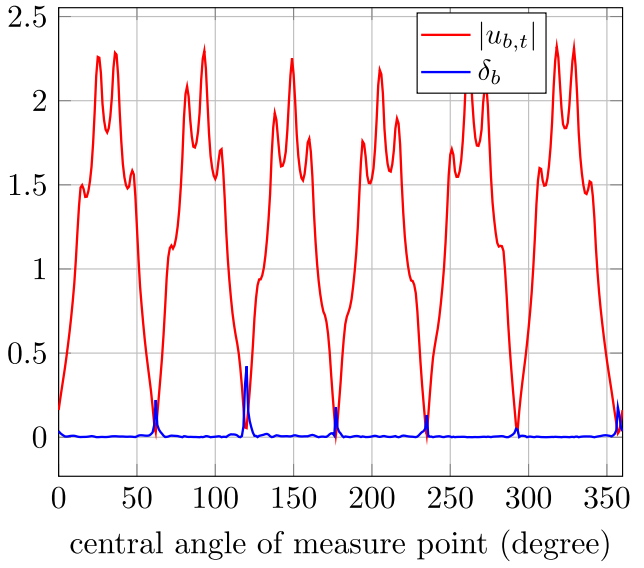

FIGURE 9. Relative error δ_b for boundary potentials computed with I_6.

the complete electrode model with different current patterns applied on the electrodes. $u_{b,t}$ and $u_{b,r}$ are the boundary potentials computed with $\sigma_{p,t}$ and $\sigma_{p,r}$, respectively. The relative error is defined as $\delta_b = \frac{|u_{b,t}-u_{b,r}|}{|u_{b,t}|}$.

The variation of $u_{b,t}$ with central angle of the observation point on the boundary is shown in Fig. 7, and the difference $|u_{b,t} - u_{b,r}|$ is in Fig. 8. It is seen that the difference between boundary potentials with $\sigma_{p,t}$ and $\sigma_{p,r}$ is very small. Specifically, the relative error δ_b is shown in Fig.9. It is close to zero save in the range where $u_{b,t}$ is approximately zero. Indeed, $|u_{b,t}|$ is the denominator in the definition of δ_b; when $|u_{b,t}|$ is about zero, a very small error in $|u_{b,t} - u_{b,r}|$ leads to a large value in δ_b.

According to (15), i.e., the relation between $\mathcal{E}(\sigma)$ and $u_{b,\epsilon} - u_b$, the noise level in $\mathcal{E}(\sigma)$ is decided by the noise in $u_{b,\epsilon} - u_b$. So, as long as the error in $u_{b,\epsilon} - u_b$ is reasonable, the power density $\mathcal{E}(\sigma)$ can be computed to retrieve the conductivity distribution with methods well developed in the literature.

C. RETRIEVAL OF σ FROM $\mathcal{E}(\sigma)$ WITH ITERATIVE METHOD

The Levenberg-Marquardt algorithm (LMA) can be used to get the conductivity distribution σ from the obtained power density $\mathcal{E}(\sigma)$, which is the 4th step in the strategy 1. To compute the power density from equation (15) calls for the knowledge of $\nu(x)$, which cannot be obtained here. Therefore, $\mathcal{E}(\sigma)$ is computed directly from its definition $\sigma|\nabla u|^2$, where u is obtained with the complete electrode model introduced in section II. The DOI is represented by 15690 triangles for the forward computation and 14301 triangles for the inversion. The complete electrode model and current patterns I^1 and I^{16} are used to compute potentials u_1 and u_{16} from the σ_r

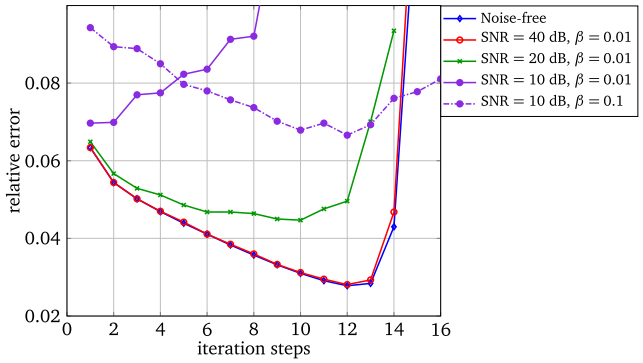

FIGURE 10. Relative error δ_b for the boundary potentials computed with I_6.

retrieved by the SVD-based method. The boundary values of u_1 and u_{16} are then used as boundary conditions in the LMA based on the continuum model.

LMA is implemented according to algorithm 2. The relative error is $\delta = \frac{\|\sigma_{p,t}-\sigma_{p,r}\|_{L_2}}{\|\sigma_{p,t}\|_{L^2}}$. One stops when $\delta < 10^{-3}$ or the number of iterations is larger than 30. Parameter α_k for the k-th iteration is $\alpha_k = \alpha_0/a^k$ with $\alpha_0 = 50.0$ and $a = 1.5$. The value of β is set as 10^{-2}, but it could be greater or smaller whether needed. A large value of β can provide a better noise tolerance of the Levenberg-Marquardt method. The result shown in Fig. 5b obtained via the SVD-based method is taken as initial guess in the iteration.

Noise is appraised with signal-to-noise ratio (SNR)

$$\text{SNR} = 20\log_{10}\frac{\|\mathcal{E}_p\|_{L_2}}{\|\mathcal{N}\|_{L_2}}, \tag{36}$$

where $\mathcal{N}$ is a Gaussian white noise distribution.

Numerical examples involve different levels of noise in the data $\mathcal{E}(\sigma)$. Fig. 11a gives the results with SNR $= \infty$, i.e., no noise in the data $\mathcal{E}(\sigma)$. Results are much better that those with the SVD-based method. But, in practice, noise is faced with. So, the noise tolerance of the Levenberg-Marquardt approach is a key factor. It is investigated by adding to the data $\mathcal{E}(\sigma)$ different levels of noise.

SNR $= 40$, 20, and 10 dB are considered. The variation of the relative error δ is given in Fig. 10. With 40 dB, LMA provides a good convergence, and the relative error decreases as fast as without noise, and quickly achieved at $\delta = 0.028$ at iteration step 12, see Fig. 11b. Afterwards, a divergence is observed, and its reason is given in the previous section.

But when the noise is increased to 10 dB, the performance of LMA worsens. However, it is observed from Fig. 11c for 20 dB that the result is still much better than the one obtained with the SVD-based method.

When SNR $= 10$ dB, in effect the method does not produce convergent results anymore, see Fig. 10, noticing that more than 30% of noise is added to the data $\mathcal{E}(\sigma)$. In this case, a better noise tolerance is required. The value of β is increased from 1×10^{-2} to 0.1, and a good convergence is observed from the dash-dotted curve in Fig. 10, the best result obtained

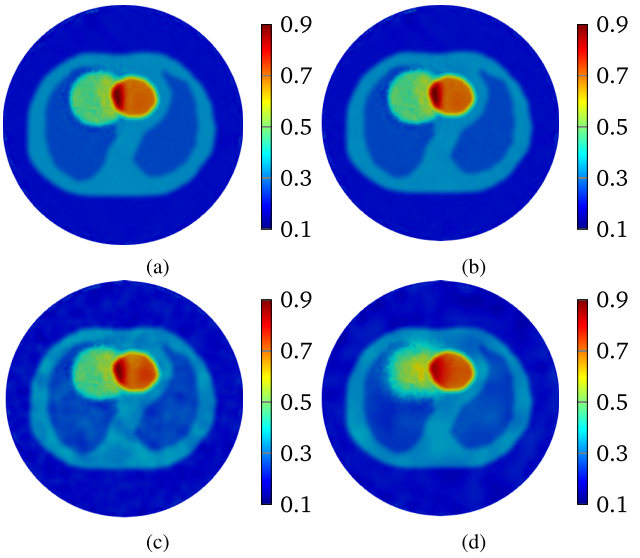

FIGURE 11. Retrieved results with Levenberg-Marquardt algorithm for different levels of noise in data $\mathcal{E}(\sigma)$: (a) noise free case; (b) with SNR = 40 dB (1% of noise); (c) 20 dB (10% of noise); (d) 10 dB (more than 30% of noise).

at step 12 being given in Fig. 11d, which is much better than with the SVD-based method.

In brief, the large value of β ensures proper noise tolerance, yet this value cannot be too large to make the algorithm converge well or to avoid over-smoothed results.

These numerical simulations show that the Levenberg-Marquardt approach provides the conductivity distribution of a closed domain with high accuracy, and has good noise tolerance. With high noise level, the conductivity can still be well mapped if proper value of β.

IV. CONCLUSION

An hybrid strategy has been proposed for acousto-electric tomography in order to retrieve the conductivity distribution of the DOI from voltages measured on electrodes attached at its boundary. How to implement this strategy has been detailed, and illustrated by comprehensive numerical simulations.

An SVD-based method is used as boundary potential reconstruction method to compute the electrical potential on the whole boundary, and it is shown that, with a low quality reconstruction of the interior perturbation of the conductivity in the DOI, the boundary potential can be computed with good accuracy. Meanwhile, good noise tolerance for achieving high-quality conductivity distribution from the power density is critical for the final result.

The iterative Levenberg-Marquardt method is used to retrieve the conductivity from the computed power density. Strong noise tolerance is observed and the quality of the final conductivity map much improves, e.g, a good retrieval with relative error less than 3% is achieved in a dozen of iterations for low-level noise, and good results are still obtained with higher-level noise.

The work summarized herein can be seen as within a continuum of investigations of AET as illustrated by the companion contribution [10]. Next, one should on the one hand focus onto higher accuracy potential reconstruction methods, and on the other hand onto comprehensive validations from experimental data in laboratory-controlled environments.

REFERENCES

[1] H. Ammari, E. Bonnetier, Y. Capdeboscq, M. Tanter, and M. Fink, "Electrical impedance tomography by elastic deformation," *SIAM J. Appl. Math.*, vol. 68, no. 6, pp. 1557–1573, Jan. 2008.

[2] P. Grasland-Mongrain and C. Lafon, "Review on biomedical techniques for imaging electrical impedance," *IRBM*, vol. 39, no. 4, pp. 243–250, Aug. 2018.

[3] T. D. C. Martins, A. K. Sato, F. S. D. Moura, E. D. L. B. D. Camargo, O. L. Silva, T. B. R. Santos, Z. Zhao, K. Möeller, M. B. P. Amato, J. L. Mueller, R. G. Lima, and M. D. S. G. Tsuzuki, "A review of electrical impedance tomography in lung applications: Theory and algorithms for absolute images," *Annu. Rev. Control*, vol. 48, pp. 442–471, 2019.

[4] S. Liu, J. Jia, Y. D. Zhang, and Y. Yang, "Image reconstruction in electrical impedance tomography based on structure-aware sparse Bayesian learning," *IEEE Trans. Med. Imag.*, vol. 37, no. 9, pp. 2090–2102, Sep. 2018.

[5] S. Liu, H. Wu, Y. Huang, Y. Yang, and J. Jia, "Accelerated structure-aware sparse Bayesian learning for three-dimensional electrical impedance tomography," *IEEE Trans. Ind. Informat.*, vol. 15, no. 9, pp. 5033–5041, Sep. 2019.

[6] M. Dai, T. Sun, X. Chen, L. Yu, M. Chen, P. Hao, X. Zeng, J. Yan, and S. Chen, "A b-scan imaging method of conductivity variation detection for magneto–acousto electrical tomography," *IEEE Access*, vol. 7, pp. 26881–26891, 2019.

[7] X. Duan, P. Koulountzios, and M. Soleimani, "Dual modality EIT-UTT for water dominate three-phase material imaging," *IEEE Access*, vol. 8, pp. 14523–14530, 2020.

[8] H. Ammari, P. Grasland-Mongrain, P. Millien, L. Seppecher, and J.-K. Seo, "A mathematical and numerical framework for ultrasonically-induced lorentz force electrical impedance tomography," *J. Math. Pures Appl.*, vol. 103, no. 6, pp. 1390–1409, Jun. 2015.

[9] N. Hyvönen and L. Mustonen, "Smoothened complete electrode model," *SIAM J. Appl. Math.*, vol. 77, no. 6, pp. 2250–2271, Jan. 2017.

[10] C. Li, M. Karamehmedovic, E. Sherina, and K. Knudsen, "Levenberg-Marquardt algorithm for acousto-electric tomography based on the complete electrode model," 2019, *arXiv:1912.08085*. [Online]. Available: http://arxiv.org/abs/1912.08085

[11] S. Hubmer, K. Knudsen, C. Li, and E. Sherina, "Limited-angle acousto-electrical tomography," *Inverse Problems Sci. Eng.*, vol. 27, no. 9, pp. 1298–1317, Sep. 2019.

[12] B. J. Adesokan, B. Jensen, B. Jin, and K. Knudsen, "Acousto-electric tomography with total variation regularization," *Inverse Problems*, vol. 35, no. 3, Mar. 2019, Art. no. 035008.

[13] G. Bal, W. Naetar, O. Scherzer, and J. Schotland, "The Levenberg–marquardt iteration for numerical inversion of the power density operator," *J. Inverse Ill-Posed Problems*, vol. 21, no. 2, pp. 265–280, Jan. 2013.

[14] J. Jossinet, B. Lavandier, and D. Cathignol, "Impedance modulation by pulsed ultrasound," *Ann. Acad. Sci.*, vol. 873, no. 1, pp. 396–407, Apr. 1999.

[15] J. Jossinet, C. Trillaud, and S. Chesnais, "Impedance changes in liver tissue exposed in vitroto high-energy ultrasound," *Physiol. Meas.*, vol. 26, no. 2, pp. S49–S58, Apr. 2005.

[16] P. Kuchment, "Mathematics of hybrid imaging: A brief review," in *The Mathematical Legacy of Leon Ehrenpreis*. Milano, Italy: Springer, 2012, pp. 183–208.

[17] X. Song, Y. Xu, and F. Dong, "Linearized image reconstruction method for ultrasound modulated electrical impedance tomography based on power density distribution," *Meas. Sci. Technol.*, vol. 28, no. 4, Apr. 2017, Art. no. 045404.

[18] E. Somersalo, M. Cheney, and D. Isaacson, "Existence and uniqueness for electrode models for electric current computed tomography," *SIAM J. Appl. Math.*, vol. 52, no. 4, pp. 1023–1040, Aug. 1992.

[19] R. A. Adams, *Sobolev Spaces*. New York, NY, USA: Academic, 1975.

[20] A. Lechleiter and A. Rieder, "Newton regularizations for impedance tomography: Convergence by local injectivity," *Inverse Problems*, vol. 24, no. 6, Dec. 2008, Art. no. 065009.

[21] A. Lechleiter and A. Rieder, "Newton regularizations for impedance tomography: A numerical study," *Inverse Problems*, vol. 22, no. 6, pp. 1967–1987, Dec. 2006.

[22] J. J. Moré, "The Levenberg-Marquardt algorithm: Implementation and theory," in *Numerical Analysis: Proceedings of the Biennial Conference Held at Dundee*. Berlin, Germany: Springer, 1978, pp. 105–116.

[23] H. Brusset, D. Depeyre, J.-P. Petit, and F. Haffner, "On the convergence of standard and damped least squares methods," *J. Comput. Phys.*, vol. 22, no. 4, pp. 534–542, Dec. 1976.

[24] M. Hanke, "A regularizing Levenberg–Marquardt scheme, with applications to inverse groundwater filtration problems," *Inverse Problems*, vol. 13, no. 1, pp. 79–95, Feb. 1997.

[25] B. Kaltenbacher, A. Neubauer, and O. Scherzer, *Iterative Regularization Methods for Nonlinear Ill-Posed Problems*. Berlin, Germany: De Gruyter, 2008.

[26] E. Kreyszig, *Introductory Functional Analysis with Applications*. Hoboken, NJ, USA: Wiley, 1978.

[27] S. Roy and A. Borzì, "A new optimization approach to sparse reconstruction of log-conductivity in acousto-electric tomography," *SIAM J. Imag. Sci.*, vol. 11, no. 2, pp. 1759–1784, Jan. 2018.

[28] Y. Capdeboscq, J. Fehrenbach, F. de Gournay, and O. Kavian, "Imaging by modification: Numerical reconstruction of local conductivities from corresponding power density measurements," *SIAM J. Imag. Sci.*, vol. 2, no. 4, pp. 1003–1030, Jan. 2009.

CHANGYOU LI (Member, IEEE) was born in Yulin, Shaanxi, China, in 1986. He received the B.S. degree in electronic science and technology and the M.S. degree in physics from Xidian University, Xi'an, China, in 2009 and 2012, respectively, and the Ph.D. degree in physics, with a Chinese Scholarship Council Grant, from the Laboratoire des Signaux et Systèmes, Centre National de la Recherche Scientifique, Gif-sur-Yvette, France, CentraleSupélec, Gif-sur-Yvette, and the Laboratoire des Signaux et Systèmes, University Paris-Sud, Orsay, France, in 2015.

From 2015 to 2016, he was a Postdoctoral Fellow with the Singapore University of Technology and Design, Singapore, where he was involved in electrical property tomography based on the measured magnetic field data. Since 2016, he has been an Associate Professor with Northwestern Polytechnical University, Xi'an, China. In 2017, he was a Visiting Postdoctoral Fellow with DTU Compute, Technical University of Denmark, Lyngby, Denmark, where he was investigating electrical impedance tomography based on a complete electrical model. He is also working on impedance/resistivity tomography, hybrid inverse problems under many guises, computational electromagnetics, especially organized/disorganized periodic structures, nondestructive testing, and inverse scattering. His current research interests include building efficient broadband and versatile computational model of multilayered fiber-based composite laminates with potential applications from eddy-current nondestructive testing to photonics and developing electromagnetic or multiphysics-based nondestructive testing methods for fiber-reinforced composites.

KANG AN was born in Handan, Hebei, China, in 1997. He received the B.S. degree in electromagnetic field and wireless technology from Northwestern Polytechnical University, Xian, China, in 2018, where he is currently pursuing the master's degree in electromagnetic field and microwave technology. He is working on acousto-electric tomography based on a complete electrical model.

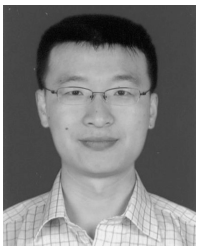

KUISONG ZHENG (Member, IEEE) received the Ph.D. degree in radio science from Xidian University, Xi'an, China, in 2006. He was an Associate Researcher with the Department of Electronic and Information Engineering, Hong Kong Polytechnic University, Hong Kong, from 2006 to 2008. He is currently an Associate Professor with the School of Electronics and Information, Northwestern Polytechnical University, Xi'an.

DOMINIQUE LESSELIER (Senior Member, IEEE) was born in Lons-le-Saunier, France, in August 1953. He received the bachelor's degree from the Ecole Supérieure d'Electricité (Supélec), Paris, France, and the Doctorat d'Etat et Sciences Physiques degree from Université Pierre et Marie Curie, Paris, in 1975 and 1982, respectively.

He has been with the Centre National de la Recherche Scientifique (CNRS), since October 1981, and he is currently the Director of the Research CNRS Emeritus. He belongs to the Laboratoire des sgnaux et systèmes, CNRS, CentraleSupélec, Université Paris-Saclay, Gif-sur-Yvette, France. He was a Visiting Scholar with the Department of Electrical Engineering, University of California at Los Angeles, Los Angeles, USA, from 1982 to 1983. As the Director, from 2006 to 2009, of the Groupement de Recherche CNRS "GDR Ondes, he managed a large network of scientists involved in the science of waves. His research interests include the development of solution imaging methods of inverse problems, from mathematics to numerics to applications, and vice versa.

Dr. Lesselier is a Fellow of the Institute of Physics and a member of the Electromagnetics Academy and of the International Union of Radio Science, Commission B. He was a recipient of the R. W. P. King Award, in 1982, from the IEEE Antennas and Propagation Society. He was on the International Advisory Panel of Inverse Problems, from 2005 to 2016, after serving on its Editorial Board, from 1997 to 2004. Since 1998, he is on the Standing Committee of the Electromagnetic Non-Destructive Evaluation Workshop Series and the International Steering Committee of the International Symposia on Applied Electromagnetics and Mechanics. Since 2003, he has been an Associate Editor of *Radio Science*.